ISSN 2075-1133, Inorganic Materials: Applied Research, 2016, Vol. 7, No. 3, pp. 330–339. © Pleiades Publishing, Ltd., 2016.
Original Russian Text © S.A. Maslyaev, E.V. Morozov, P.A. Romakhin, V.N. Pimenov, V.A. Gribkov, A.N. Tikhonov, G.G. Bondarenko, A.V. Dubrovsky, E.E. Kazilin, I.P. Sasinovskaya, O.V. Sinitsyna, 2015, published in Fizika i Khimiya Obrabotki Materialov, 2015, No. 3, pp. 5–17.

EFFECTS OF ENERGY FLUXES ON MATERIALS

Damage of Al_2O_3 Ceramics under the Action of Pulsed Ion and Plasma Fluxes and Laser Irradiation

S. A. Maslyaev[a], E. V. Morozov[a, b], P. A. Romakhin[a, c], V. N. Pimenov[a], V. A. Gribkov[a, d], A. N. Tikhonov[c], G. G. Bondarenko[c], A. V. Dubrovsky[a], E. E. Kazilin[a], I. P. Sasinovskaya[a], and O. V. Sinitsyna[e]

[a] *Baikov Institute of Metallurgy and Materials Science, Russian Academy of Sciences, Leninskii pr. 49, Moscow, 119991 Russia*
e-mail: maslyaev@mail.ru, lieutenant@list.ru, oblivion-007@mail.ru, pimval@mail.ru, gribkovv@rambler.ru, adubrov@mail.ru, symp@imet.ac.ru, porfirievna@mail.ru

[b] *Moscow State Industrial University, ul. Avtozavodskaya 16, Moscow, 115280 Russia*

[c] *National Research University Higher School of Economics, ul. Myasnitskaya 20, Moscow, 101000 Russia*
e-mail: atikhonov@hse.ru, gbondarenko@hse.ru

[d] *Institute of Plasma Physics and Laser Microfusion, Hery Str. 23, Warsaw, 01-497 Poland*

[e] *Nesmeyanov Institute of Organoelement Compounds, Russian Academy of Sciences, ul. Vavilova 28, Moscow, 119991 Russia*
e-mail: sinitsyna@gmail.com

Received December 15, 2014; in final form, January 11, 2015

Abstract—The effects of powerful pulsed ion and high-temperature plasma fluxes generated in a plasma focus (PF) device and the effect of free running laser radiation on a corundum (α-Al_2O_3) ceramic produced by powder technology are studied. The power flux density q and acting pulse time τ for plasma stream, ion flux, and laser irradiation were $q_p \approx 10^7$ W/cm^2 and $\tau_p \approx 100$ ns, $q_i \approx 10^8$ W/cm^2 and $\tau_i \approx 20$ ns, and $q_l \approx (3–5) \times 10^5$ W/cm^2 and $\tau_l \approx 0.7$ ms, respectively. The resistance of the ceramic to pulsed energy fluxes was estimated by the weight loss of irradiated specimens and by the surface layer defects (damage). The combined use of PF and pulsed laser irradiation is shown to allow simulation of the extreme erosion and damage of materials in thermonuclear fusion facilities (such as ELM effects in ITER or at the first wall of inertial confinement chambers).

Keywords: pulsed ion and plasma streams, plasma focus, laser irradiation, material erosion, material damage, thermonuclear fusion reactor

DOI: 10.1134/S2075113316030151

INTRODUCTION

At the present time, high-strength alumina ceramics with corundum structure ([α-Al_2O_3) are widely used for manufacture of constructional components applied in various mechanical engineering fields, electronics, and aerospace engineering. This is due to the fact that, besides high mechanical strength, this material possesses many other useful properties, such as high hardness, heat and wear resistance, thermal conductivity, good insulation characteristics, and others. Being a part of electronic equipment as a substrate material for microcircuits and large-scale integrated circuit packages, Al_2O_3-based ceramic can sustain considerable radiation and thermal loads, which allows one to place equipment on the outer side of spacecrafts. These loads can be both pulsed actions (e.g., from solar flares or micrometeoroid impacts) and long-term exposures (solar-wind flux or heating during entry into dense atmosphere).

In [1], Al_2O_3 ceramic was considered along with boron nitride (BN) as a promising coating material for antenna coils placed inside the discharge chamber of MAST (Mega Ampere Spherical Tokamak) [2]. Typically, among important factors acting on the material facing the fusion plasma are effects developing in the edge region of the tokamak plasma upon its contact with the material (so-called edge localized modes or ELM effects). These effects last for $\leq 10^{-3}$ s and occur with a frequency of ~50–100 Hz to result in material damage owing to a high (up to 1 MJ/m^2) heat load, at which the instantaneous power density reaches $q \approx 10^5$ W/cm^2 [2, 3]. Along with ELMs effects, rarer but more destructive phenomena can occur in tokamaks, among which are vertical displacements of plasma (VDE) and disruption instability causing pulsed heat fluxes up to 10^2 MJ/m^2 acting on the material.

The possibility of harsh heat loads requires special tests to determine the heat resistance of Al_2O_3 to extreme power fluxes. However, to date, there have been few such experiments performed in Russia and

Table 1. Parameters of pulsed action of radiation on the Al_2O_3 ceramic samples

Radiation type	Energy density E, J/cm^2	Pulse time τ, s	Power density q, W/cm^2	Damage factor* F, W cm^{-2} s$^{1/2}$
PF plasma	10^0	10^{-7}	10^7	3.3×10^3
PF ion flux	10^1	2×10^{-8}	5×10^8	7×10^4
Laser radiation	3.4×10^2	0.7×10^{-3}	4.9×10^5	1.3×10^4
	2×10^2		2.9×10^5	7.7×10^3

* F is the damage factor of irradiated material $F = q\tau^{0.5}$ [7].

other countries. Let us mention the work [1] where comparative tests of boron nitride and alumina films with a thickness of ~20 μm grown on a pure aluminum support in plasma focus devices on exposure to pulsed fluxes of fast ions and high-temperature plasma (HTP) were performed. In [4], the optical properties of artificial sapphire, quartz, and topaz after irradiation with microsecond pulsed ion-plasma beams with a hydrogen ion energy of ~60 keV were studied. However, Al_2O_3 ceramic prepared by the powder technique has not been studied until now under the action of pulsed power fluxes.

The aim of the present work was to study the effect of intense pulsed power fluxes (fast deuterons and high-temperature deuterium plasma generated in a PF-5M device), as well as the effect of free running Nd-glass laser radiation (LR) on α-Al_2O_3 ceramic samples prepared by the powder metallurgical technique. The main attention was given to estimation of the resistance of the material to the radiation-heat action of powerful ion and plasma beams, as well as laser beams. Such exposures were used to analyze and simulate the extreme erosion and damage processes of materials occurring in magnetic confinement controlled-fusion reactors (such as ELM effects in ITER [2, 3]), as well as in inertial confinement fusion reactors (such as the National Ignition Facility (NIF), Lawrence Livermore National Laboratory, United States).

MATERIALS AND METHODS

The material under study was an Al_2O_3 ceramic with corundum structure. The Al_2O_3 powder was prepared by ultrasonic spray pyrolysis [5]. The samples were molded by uniaxial compression using an organic binder based on polyvinyl alcohol under the pressure of 100 MPa followed by sintering in air for 2 h at 1200°C. The samples for irradiation have the shape of right-angle prism with dimensions of $40 \times 4 \times 4$ mm or $12 \times 4 \times 4$ mm.

The samples were irradiated with pulsed fast ion and HTP beams in a PF-5M plasma focus device [6] using nitrogen and air as working gases. The chamber pressures of nitrogen and air were ~270 and ~300 Pa, respectively. The peak energy of PF battery was 2 kJ. The samples were placed at the distance of 8 cm from the anode along the PF chamber axis; the highest radiation was in the central section of samples with an area of ~12×4 mm^2; i.e., the irradiation intensity in long targets decreased upon moving away from the sample center to its periphery and the irradiation intensity in short targets remained virtually the same throughout the surface under irradiation.

The samples were irradiated with laser pulses in air on a GOS 1001 device ($\lambda = 1.06$ μm) in the free running mode. The laser light was concentrated in defocused focal spots of a lens with diameters of 0.43 and 0.57 cm. The parameters of irradiation of samples in the plasma and laser devices are given in Table 1.

As seen, the energy density E in the laser pulse was one to two orders of magnitude higher than that upon irradiation of the target in the PF device; however, the power density q upon ion and plasma irradiation in the PF was the same order of magnitude higher than that upon longer term laser irradiation. The damage factor F was approximately identical in both cases.

The samples under irradiation were studied by UV-visible spectroscopy, scanning electron microscopy, and atomic force microscopy, as well as by X-ray spectral analysis and X-ray powder diffraction (XRPD).

RESULTS AND DISCUSSION

Material Erosion upon Irradiation

The ion-plasma and laser irradiation of Al_2O_3 ceramic was found to cause erosion of the material, which was detected by a decrease in the weight of the target sample and caused mainly by evaporation of the surface layer upon laser irradiation, as well as by its sputtering by ion and plasma streams upon irradiation in PF. The weight loss on exposure to laser radiation was found to be more significant than that under pulsed ion-plasma action, which was likely caused by heating of the target substance to a higher temperature upon irradiation in the PF, providing a higher power flux density. Since the target substance under evaporation is heated to a higher temperature, its scattering velocity is considerably higher than that upon evaporation on exposure to a more powerful laser beam. The calculations show that, in our experiments, the scattering velocity v of the laser-evaporated substance is ~10^6 cm/s, whereas when the target is exposed to the

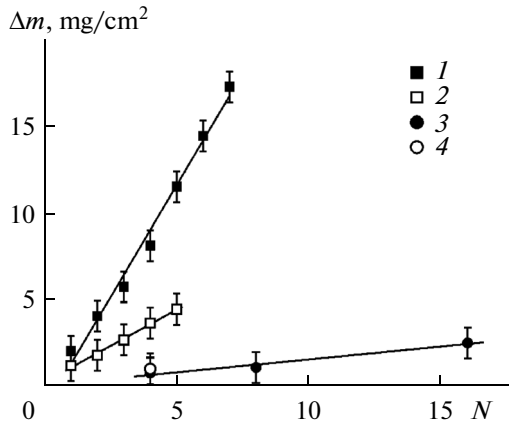

Fig. 1. Specific weight loss of the Al_2O_3 ceramic samples (per unit area of irradiated surface) as a function of the number of radiation pulses N for laser irradiation at the power density of $q = 4.87 \times 10^5$ (*1*) and 2.83×10^5 W/cm^2 (*2*) and for PF plasma-beam irradiation in the nitrogen plasma (*3*) and air mixture (*4*).

plasma beam in the PF, the scattering velocity is $v = 4 \times 10^6$ cm/s, i.e., fourfold higher. Thus, the radiation energy in the PF experiments being converted to the kinetic energy of scattered substance $mv^2/2$ is redistributed in favor of the increase in the scattering velocity v and the decrease in the evaporated target weight m compared to the case with laser irradiation.

Figure 1 shows the average weight loss Δm per unit surface of the irradiated Al_2O_3 ceramic samples as a function of the number of laser pulses N for two values of the radiant power density q and ion-plasma action in the PF. As one can see, the weight loss Δm of the sample increases linearly with an increase in N, the Δm value upon laser action increasing significantly with an increase in q. The average thickness of layer h evaporated within one laser pulse increases correspondingly (Table 2): the value of h is about 2 μm at the lowest power density of $q \approx 2.9 \times 10^5$ W/cm^2 and increases to ~6 μm at $q \approx 4.9 \times 10^5$ W/cm^2. In the PF, the thickness of the layer evaporated within one pulse was $h \approx 0.4$ μm using air as the plasma-forming gas and ~0.6 μm in a nitrogen plasma.

It should be noted that evaporation of the target material located in the cathode zone of the PF working chamber is typically accompanied by its deposition of the anode material evaporated by a powerful electron beam and, in some cases, deposition of other working chamber materials onto the surface under irradiation [7, 8].

This process, resulting frequently in underestimation of the evaporated target weight loss, played no significant role in our experiments, since the PF-5M device uses a hollow anode made of stainless steel (in contrast to commonly used copper). In such a design, the anode material evaporated by the electron beam is deposited onto its internal wall and hardly falls on the target.

Despite a significant difference in the h and v values typical of erosion of the ceramic upon laser irradiation and ion-plasma irradiation, the damage factor F for the processing parameters under comparison differs insignificantly (Table 1). This means that this parameter characterizes the material damage associated with the formation of surface structure defects (pores, droplets, beads, microcracks, and the like) and the formation of the surface relief pattern after irradiation to a greater degree compared to erosion caused by the weight loss upon evaporation.

It should be noted that the laser radiation energy is transmitted to the electronic subsystem in a thin surface skin layer with a thickness $\delta \ll \lambda$, i.e., much less than 1 μm [9]. This action occurs for a long time period of ~1 ms in discontinuous manner, since the free running laser operates in a "spiking mode." In the time of each spike, the energy in this thin layer is transmitted from electrons to the crystal lattice of target material and the layer under consideration evaporates during this time. Thus, within the time of a laser pulse, the target substance evaporates and scatters many times at a quite high rate (~10^6 cm/s).

Upon ion irradiation, the fast ions flux with an energy of 100 keV and higher (in particular, nitrogen ions in aluminum) directly transmits its energy mainly to the solid lattice at the depth of ~100 nm [10] with the so-called Bragg absorption peak at the end of the path. Compared to laser irradiation, this process occurs within a significantly shorter time interval (from 10^{-7} to 10^{-8} s); therefore, a high volumetric power density is created in the absorbing layer of the substance, its temperature increases dramatically, and the substance scatters with a velocity fourfold higher than that upon laser action. In addition, the duration of a pulse of fast ion flux is shorter than the time of inertial confinement of the heated substance (plasma spread time), and the energy of incident ion flux transforms mainly to the kinetic energy of evaporated par-

Table 2. Estimation of the average weight loss and the thickness of evaporated layer of Al_2O_3 ceramic upon laser action

Distance from lens to sample L, cm	Irradiated spot diameter d, cm	Irradiated spot area S, cm^2	Power density q, W/cm^2	Average weight loss per pulse Δm, mg	Average thickness of layer evaporated per pulse h, μm
45.2	0.43	0.145	4.87×10^5	0.343	5.89
43.7	0.57	0.25	2.83×10^5	0.225	2.24

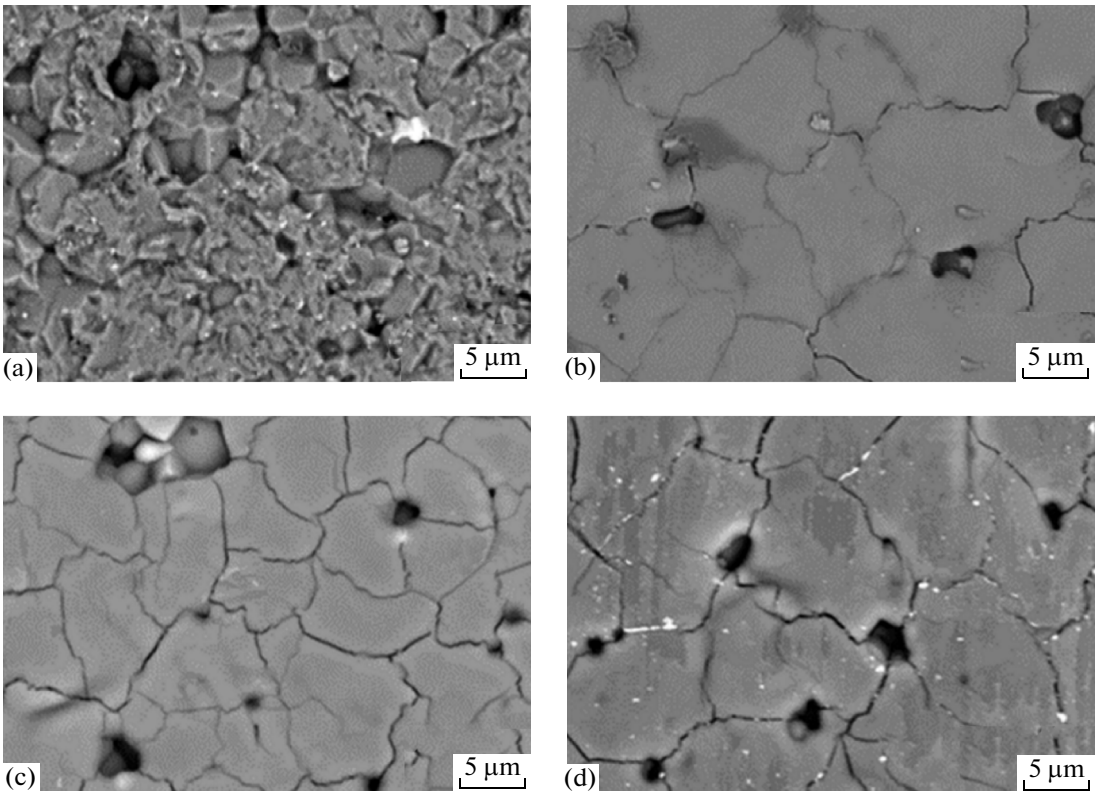

Fig. 2. Microstructure of the Al_2O_3 ceramic after irradiation with nitrogen ions and nitrogen plasma: (a) initial and at the number of radiation pulses (b) $N = 1$, (c) $N = 2$, and (d) $N = 4$.

ticles and the weight of the evaporated layer is relatively low.

As a comparison, note that, under deuterium plasma irradiation in the PF at a higher power density ($q \approx 10^9$–10^{11} W/cm^2), the Al_2O_3 compound grown on a pure aluminum substrate evaporates at the rate of ~4 μm/pulse [1]. Irradiation of the CFC/SiC ceramic (carbon-fiber-based composite material reinforced with silicon carbide (SiC) particles) under the same conditions was accompanied by a lower erosion (~2–2.5 μm/pulse) and irradiation of the boron nitride (BN) ceramic was accompanied by a higher erosion (~6 μm/pulse) [1]. The erosion of Eurofer97 ferritic-martensitic steel as well as that of tungsten upon irradiation with deuterium ions and deuterium plasma with a power density of $q \approx 10^{10}$–10^{11} W/cm^2 was ~2 μm/pulse [11].

These data show that the Al_2O_3 ceramic under study possesses almost the same erosion resistance to powerful pulsed ion and plasma streams as known ceramic and metallic materials promising for application in thermonuclear power engineering [12–16].

Surface Layer Damage upon Irradiation in PF

Figures 2 and 3 show the surface layer microstructure of Al_2O_3 ceramic samples after irradiation in the PF device in the nitrogen and air atmosphere. As seen, after exposure of the target to fast ions of plasma-forming gas and HTP, the surface layer displays the formation of structural defects, such as pores, shells, and microcracks forming a mesh network whose meshes are arranged along the whole irradiated surface and have predominantly equiaxial shape. The typical mesh size Φ is from 4 to 20 μm and hardly depends on the number of irradiation pulses N. In the central zone of irradiation, where the ion stream dominates over the HTP stream [17, 18], the Φ value is from 4 to 10 μm and, at the periphery of samples where the effect of plasma streams has a dominant role, the mesh size increases slightly to 15–20 μm. The mesh boundaries display pores whose mean size is ~1–2 μm and also depends weakly on N.

The weak dependence of the pore size on the number of irradiation pulses makes it possible to assume that the pore concentration in the surface layer is defined by two processes. One process is associated with the removal of pores from a thin (less than 1 μm) layer together with the evaporated material at each impacting pulse. The second process includes the step of nucleation and growth of pores in the formed melt layer owing to the presence of gas-forming elements therein (mainly, oxygen appearing in the ceramic and evolving upon dissociation of oxide, as well as implanted nitrogen, carbon impurities, etc.). In combination, both processes prevent a noticeable increase

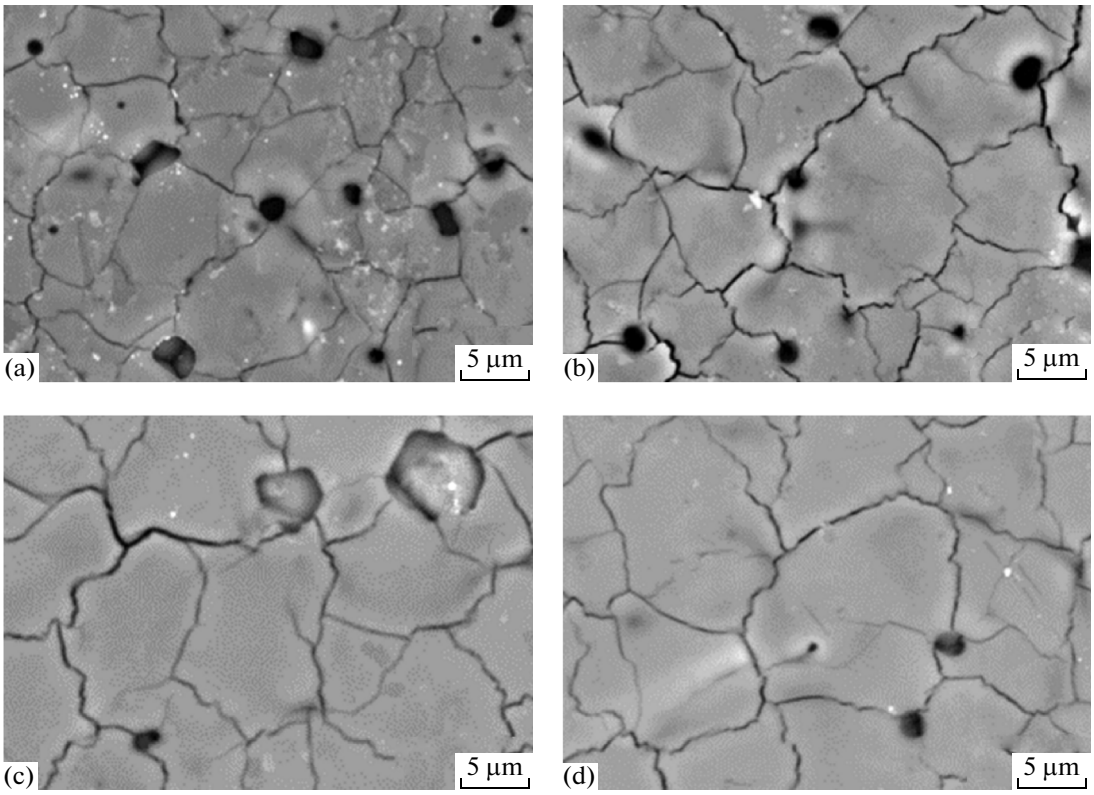

Fig. 3. Microstructure of the Al_2O_3 ceramic after irradiation with gas ions as a component of air and with air plasma at the number of radiation pulses (a) $N = 1$, (b) $N = 2$, (c) $N = 8$, and (d) $N = 16$.

in the pore size with an increase in N. The estimates show that the average number of pores per unit area is $(1.5–3.5) \times 10^5$ cm^{-2} in the central irradiation zone and increases by an order of magnitude to $(1.5–3.8) \times 10^6$ cm^{-2} at its periphery, which is due to the decrease in the erosion rate of the target sample in the zone under consideration. The average pore size is defined by the lifetime of the liquid phase in the surface layer after pulsed energy deposition, during which pores form and grow.

The presence of pores in the surface layer, which are typically stress concentrators, promotes the observed cracking after crystallization of the melt, as well as the formation of microstructure with typical arrangement of pores at the microcrack lines along the mesh boundaries as shown in Figs. 2 and 3. This phenomenon is particularly noticeable in the central irradiation zone of the samples exposed to the most intense power flows. The emergence of microcracks results from thermal tensile stresses at a high hardening rate of the liquid phase ($\sim 10^6–10^7$ deg/s) whose values exceed the tensile strength of the material. As our results show, this phenomenon depends weakly on the number of pulses N, since it is defined completely by the cooling conditions of the target sample, which remain virtually unchanged in each series of irradiation experiments. However, the above-noted change in the average mesh size in the central irradiation zone of the target suggests that the value of thermal stresses in the surface layer is not homogeneous and most likely reaches a maximum in the central irradiation zone, where the density of power flux acting on the material is the highest. One can assume that the formation of surface microcracks will have a negative effect on the physical and mechanical corrosion and other properties of the surface layers of the ceramic under study on exposure to plasma-ion power fluxes.

Damage of the Surface Layer upon Pulsed Laser Irradiation

Figure 4 shows the microstructure of surface layer of Al_2O_3 ceramic samples after exposure to pulsed laser irradiation in the free running mode. The pattern of observed structural defects, looking like a mesh network of microcracks containing pores at the mesh boundaries, is close to that after irradiation of the samples in the PF device. However, a significant difference is the fact that, with an increase in the number of laser pulses N, there is a noticeable (severalfold) increase in the average pore size, which is not observed in the PF experiments. In other words, the structure considered after exposure to laser irradiation contains pores having typical sizes of ~1–2 μm at $N \geq 1$ and ~4–6 μm at $N > 1$. This difference is due to different conditions of thermal action on the material upon pulsed irradiation

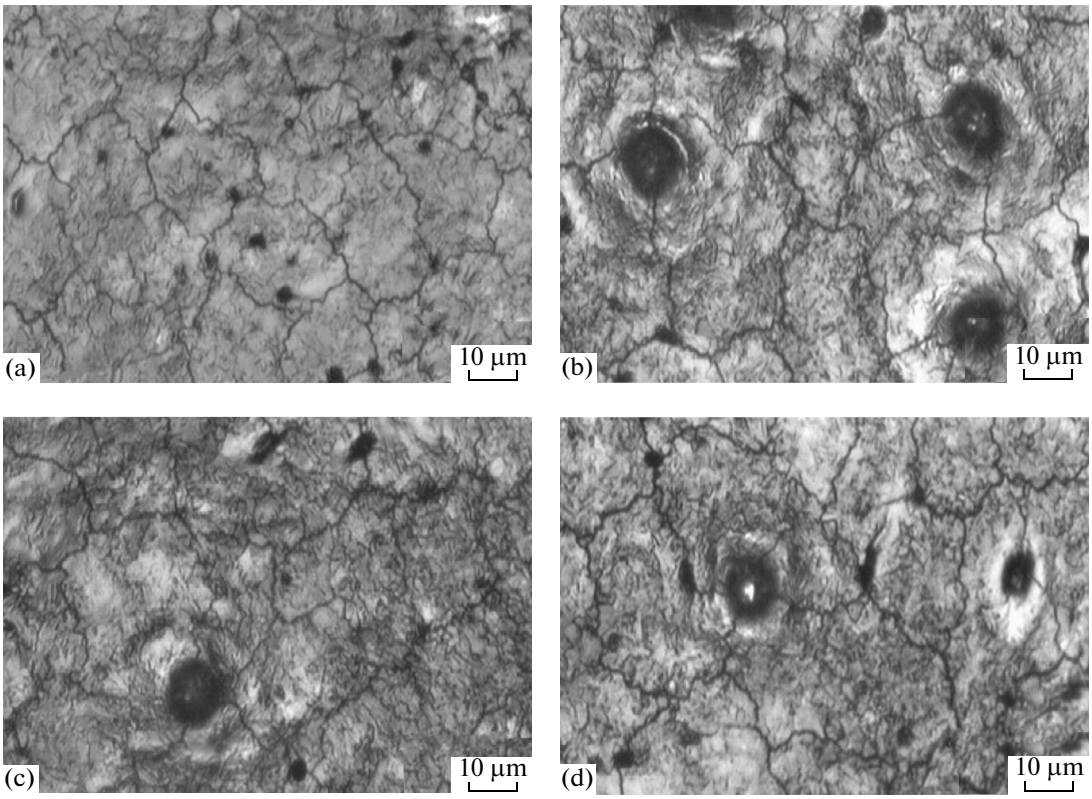

Fig. 4. Microstructure of the surface layer of the Al_2O_3 ceramic after laser irradiation at $q = 10^6$ W/cm^2 and the number of radiation pulses (a) $N = 1$, (b) $N = 2$, (c) $N = 4$, and (d) $N = 8$.

in the laser and plasma devices. At a slightly higher power density of laser pulse and significantly longer (by about four orders of magnitude) time of laser action on the target, the lifetime of the liquid phase on the ceramic surface exposed to laser irradiation was longer than that upon ion-plasma irradiation in the PF, which favored a longer term growth of pores to coarser sizes (several μm).

Surface Relief

Figure 5 shows the photomicrographs and profile records for the regions of the surface layer of Al_2O_3 ceramic in the initial state and after irradiation experiments in the plasma and laser devices.

The analysis showed that fluctuations in the surface relief level between the maximum and minimum values (the highest peak-to-valley height h_0) are from 200 to 1000 nm for the starting ceramic and vary from $h_0 \approx$ 400–2000 nm (PF) to $h_0 \approx$ 600–900 nm (LR) after irradiation in PF and LR under comparable conditions. In other words, irradiation of the ceramic in the PF device with ion and plasma streams results in the formation of a wavelike surface with a higher amplitude of surface relief fluctuations than that in the initial state.

This is due to intense explosive melting of the surface layer and subsequent vigorous boiling of the liquid phase, which result in deformation of the relief and fixation of this state under conditions of ultrafast melt quenching. It follows from the data obtained that surface melting on exposure to the free running pulsed LR occurs with a lower amplitude oscillations of waves of the surface relief, which results in smoothing of the relief compared to the initial state. This is caused by milder conditions of laser irradiation of the ceramic target, upon which a slightly higher density of incident energy is transmitted to the sample within a significantly longer time compared to the PF conditions. In this case, melting and evaporation of the surface layer proceed less intensely.

Surface Layer Distribution of Elements

The elemental analysis of the irradiated Al_2O_3 ceramic samples showed that laser irradiation in air resulted in no noticeable change in the surface layer contents of elements. At the same time, irradiation of the samples in the PF device favored redistribution of elements of the ceramic and change in the composition of the surface layer (Table 3).

Two facts come to our attention: the absence of the main implanted element, nitrogen, in the irradiated samples and the presence of carbon in noticeable amounts therein. Taking into account the data on evaporation of the ceramic, the former is explained by

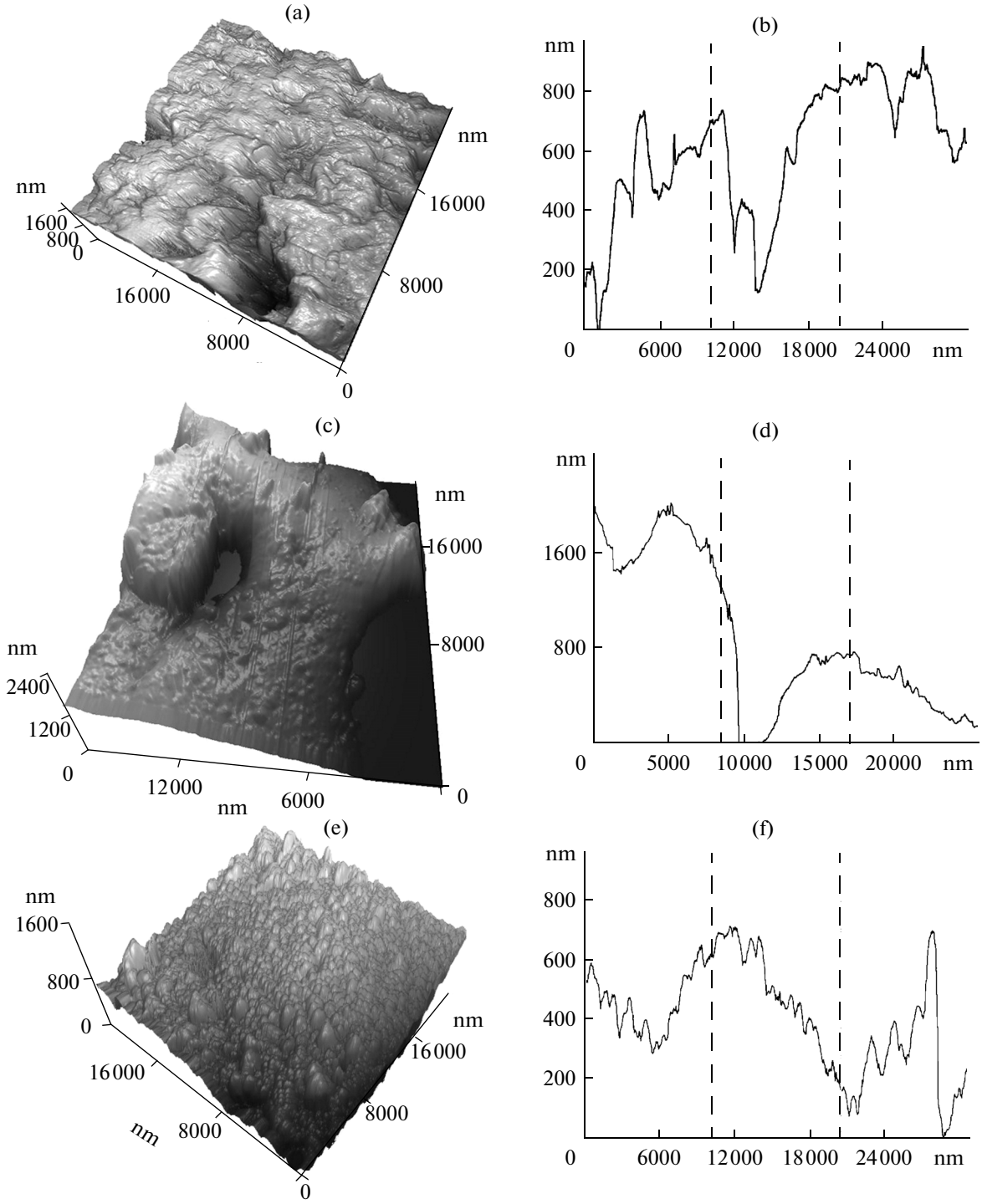

Fig. 5. AFM photomicrographs (a, c, e) and relief profile records (b, d, f) for regions of the surface layer of the Al_2O_3 ceramic in the initial state (a, b), after irradiation with nitrogen ions and one pulse of nitrogen plasma in the PF device (c, d), and after one pulse of laser radiation (e, f).

the fact that the depth of the projective path of nitrogen ions $R(N_2)$ in Al_2O_3 is not more than the thickness h of the layer evaporated per radiation pulse, i.e., $R(N_2) \le h$. For example, at the energy of fast nitrogen ions $E \approx 100$ keV, the $R(N_2)$ value is about 200 nm [19], which is considerably less than the thickness of the layer evaporated per pulse. That is to say, the layer of ions of plasma-forming gas implanted into the ceramic evaporates completely in each pulse of energy deposition. In addition, as Table 3 shows, both ele-

Table 3. Elemental composition of the surface layer in the central section of the Al_2O_3 ceramic sample upon PF irradiation (at %)

Plasma-forming gas	Number of irradiation pulses, N					
	Initial	1	2	4	8	16
Nitrogen	Al—40	Al—53	Al—42	Al—49	–	–
	O—60	O—47	O—58	O—51		
Air	Al—40	Al—51	Al—36	Al—47	Al—38	Al—40
	O—60	O—49	O—54	O—48	O—55	O—53
			C—10	C—5	C—7	C—7

ments of the ceramic evaporate upon single pulse action, but the oxygen atoms leave the surface at a high rate, which results in a noticeable shift of the starting composition of the surface-adjacent layer in favor of a higher Al concentration.

Upon subsequent pulsed treatment, there is a tendency to the recovery of the initial ratio between the components of the ceramic, the O_2 content in the surface layer increases, and the Al concentration decreases. This can be due to redistribution of the components in the concentration, temperature, and thermal stress gradient fields created by powerful pulsed energy actions.

The emergence of carbon in the surface layer of the ceramic after irradiation in the PF can be caused by two mechanisms. One of them can be due to partial diffusive penetration of carbon through the irradiated Al_2O_3 surface from the working gas atmosphere, which contained carbon dioxide (CO_2). The second mechanism typical of sample irradiation in the PF is associated with possible carbon evaporation from the surface of the PF working chamber material followed by its deposition on the surface of the ceramic under treatment. One should note the absence of other elements (Fe, Cr, and Ni) in the composition of the working chamber and anode materials appearing in the irradiated ceramic, which could interact with constituent elements after evaporation and deposition on the target surface under certain conditions as was the case for iron- and titanium-based alloys [20]. This fact emphasizes the chemical inertness of the studied ceramic under the implemented conditions of irradiation compared to metallic materials.

Simulation of Processes in Thermonuclear Facilities

The PF devices were shown earlier [7, 11] to be promising for simulation of the interaction conditions between plasma and thermonuclear reactor core materials. In particular, it was noted that the effects developing at the plasma edge on its contact with material (ELM effects) in ITER are characterized by the damage factor $F = q^{0.5}$ varying from $\sim 1.4 \times 10^4$ to 3×10^5 W cm^{-2} s$^{1/2}$ for divertor sheets and from $\sim 2 \times 10^3$ to 10^4 W cm^{-2} s$^{1/2}$ for the first wall. In the present work, the values of $F \approx 3 \times 10^3$ W cm^{-2} s$^{1/2}$ for plasma streams, $F \approx 7 \times 10^4$ W cm^{-2} s$^{1/2}$ for fast ion fluxes, and $F \approx 10^4$ W cm^{-2} s$^{1/2}$ for laser action were obtained in experiments on PF irradiation of Al_2O_3 ceramic (Table 1). Hence, it appears that, in our experiments, the F value is close to that in ITER; however, it should be noted that simulation of ELM effects using PF devices and laser action have unique features. In the former case, the important advantage of PF is that the material can be exposed to the same ion and radiation fluxes as in the case of ELM effects, and plasma disruption in ITER can be simulated under similar conditions of pulsed irradiation (although the present work uses plasma-forming gases other than those used in ITER). Among the drawbacks of this simulation method is a very short pulse time of plasma-beam action on the material in the PF, which is four orders of magnitude shorter than the duration of ELM effects.

At the same time, the aforementioned disadvantage is absent upon simulation using LR, whose advantage is the closeness between the time of pulsed action on the target sample in the free running mode ($\sim 10^{-3}$ s) and the time of plasma interaction with the substance upon ELM effects [2, 3]. However, this simulation method contemplates simulation of only heat load on the target and excludes the possible effects of ion-plasma action and accompanying processes on the sample, where among such processes are radiation sputtering of the target material, implantation of the working gas ions into the material, and formation of radiation defects. This drawback narrows the possibility of stand-alone application of laser simulation in the case under consideration, since it allows no complete simulation of radiation damage of the material under its operating conditions in the fusion reactor chamber.

Hence, it follows that the combined use of the PF and pulsed free running LR devices with corresponding selection of the target material and irradiation conditions is promising for simulation of processes of interaction between fusion plasma and working chamber materials of fusion reactors, such as ITER. This approach using exposure of the target to powerful ion and plasma beams along with independent irradiation of the target with pulsed laser beams provides a more objective presentation of the radiation resistance and damage pattern of materials irradiated with powerful fluxes, which is of prime importance for the study and

prediction of the behavior of various materials on exposure to pulsed ion and plasma streams in nuclear fusion facilities.

CONCLUSIONS

1. Irradiation of the corundum-structure (α-Al_2O_3) ceramic prepared by the powder technique with free running laser radiation fluxes ($q \approx (3–5) \times 10^5$ W/cm^2 and $\tau \approx 0.7$ ms), as well as nanosecond ion and plasma pulses (PF-6 plasma focus device, $q \approx 10^7–10^8$ W/cm^2), is accompanied by a noticeable erosion of the material. The weight loss upon laser irradiation is higher than that upon ion and plasma irradiation: the thickness of the layer of material evaporated in one pulse in the PF device is ~0.4 and ~0.6 μm in the air and nitrogen plasma, respectively, and is 4–10 times larger upon laser irradiation. After exposure to the laser, the irradiated surface has smoother relief.

2. The erosion resistance of the ceramic to the powerful pulsed ion and plasma streams simulating the operating conditions in fusion reactors is comparable with that of other ceramic and metallic materials, such as CFC/SiC carbon-fiber-based composite material, boron nitride, EuroFer97 ferritic-martensitic steel, and tungsten.

3. The damage pattern of the ceramic under study on exposure to plasma and fast ions fluxes and laser radiation is almost identical and is manifested in the formation of mesh network of microcracks and pores located mainly at the mesh boundaries. Upon laser treatment, the average pore size increases with increases in the number of radiation pulses and the power flux density.

4. The application of powerful pulsed ion and plasma beams, as well as laser irradiation, is shown to be promising for simulation of the extreme material erosion and damage processes occurring in magnetic and inertial confinement fusion reactors. Upon the corresponding selection of pulsed plasma-beam exposure conditions, irradiation in the plasma focus device adequately simulates the conditions of radiation and heat loads acting on the material in inertial confinement fusion reactors, such as NIF. In free running laser devices, the parameters of long-term heat action are found to be the closest to the conditions realized in magnetic confinement fusion reactors. Simulation of the radiation damage of the material on exposure to ion and plasma streams can be achieved in this case by the simultaneous use of PF devices.

ACKNOWLEDGMENTS

The authors are grateful to Prof. A. G. Kolmakov for providing the Al_2O_3 ceramic samples.

This work was financially supported by the International Atomic Energy Agency (IAEA CRP grant nos. 16954, 16955, 16956, 16960, and 17167).

REFERENCES

1. Gribkov, V.A., Tuniz, C., Demina, E.V., Dubrovsky, A.V., Pimenov, V.N., Maslyaev, S.V., Gaffka, R., Gryaznevich, M., Skladnik-Sadowska, E., Sadowski, M.J., Miklaszewski, R., Paduch, M., and Scholz, M., Experimental studies of radiation resistance of boron nitride, C2C ceramics Al_2O_3 and carbonfiber composites using a PF-1000 plasma–focus device, *Phys. Scr.,* 2011, vol. 83, p. 045606. doi 10.1088/0031-8949/83/04/045606
2. Kirk, A., Koch, B., Scannell, R., Wilson, H.R., Counsell, G., Dowling, J., Herrmann, A., Martin, R., and Walsh, M., Evolution of filament structures during edge-localized modes in the MAST Tokamak, *Phys. Rev. Lett.*, 2006, vol. 96, p. 185001.
3. Loewenhoff, Th., Hirai, T., Keusemann, S., Linke, J., Pintsuk, G., and Schmidt, A., Experimental simulation of edge localized modes using focused electron beams-features of a circular load pattern, *J. Nucl. Mater.*, 2011, vol. 415, pp. S51–S54.
4. Gribkov, V.A., Ivanov, L.I., Maslyaev, S.A., Pimenov, V.N., Sadowski, M.J., Skladnik-Sadowska, E., Banaszak, A., Kopec, G., Cheblukov, Yu.N., Kozodaev, M.A., Suvorov, A.L., and Smirnov, I.S., On the nature of changes in the optical characterization produced in sapphire on its irradiation with a pulsed powerful stream of hydrogen ions, *Nukleonika,* 2004, vol. 49, no. 2, pp. 43–49.
5. Antipov, V.I., Vinogradov, L.V., Goncharova, L.S., and Kolmakov, A.G., New technology for nanostructured microsphere powders production, in *Proc. 2nd Int. Conf. "Deformation and fracture of materials and nanomaterials (DFMN-2007),"* Moscow, 2007.
6. Dubrovsky, A.V., Gribkov, V.A., Pimenov, V.N., and Scholz, M., Comparative characteristics of four small dense plasma focus devices, in *Proc. 17 IAEA Technical Meeting on Research Using Small Fusion Devices*, Lisbon, Portugal, 2007; Varandas, C. and Silva, C., Eds., *AIP Conf. Proc.*, 2008, vol. 996, pp.103—107. http://dx.doi.org/10.1063/1/2916996.
7. Pimenov, V.N., Maslyaev, S.A., Demina, E.V., Ivanov, L.I., Kovtun, A.V., Gribkov, V.A., Dubrovskiy, A.V., and Ugaste, Yu.E., Effect of powerful energy flows of surface of pipe from aluminum alloy, *Perspekt. Mater.,* 2006, No. 4, pp. 43–52.
8. Pimenov, V.N., Maslyaev, S.A., Demina, E.V., Kovtun, A.V., Sasinovskaya, I.P., Gribkov, V.A., and Dubrovskiy, A.V., Interaction of powerful energy flows with tungsten surface in the "Plasma focus" setup, *Fiz. Khim. Obrab. Mater.*, 20087, No. 3, pp. 5–14.
9. Libenson, M.N., Yakovlev, E.B., and Shandybina, G.D., *Interaction of Laser Radiation with Matter. 1. Absorption of Laser Radiation by Matter,* St. Petersburg, St. Petersburg State Univ., 2008.
10. Sadiq, M., Ahmad, S., Waheed, A., and Zakaullah, M., The nitriding of aluminum by dense plasma focus, *Plasma Sources Sci. Technol.,* 2006, vol. 15, pp. 295–301.
11. Ivanov, L.I., Pimenov, V.N., and Gribkov, V.A., Interaction of power pulsed fluxes of energy with materials, *Fiz. Khim. Obrab. Mater.*, 2009, No. 1, pp. 23–37.

12. Belyakov, V., Mazul, I., and Strebkov, Yu., Manufacturing and testing of large-scale mock-ups of ITER plasma facing components in Russia, *Fusion Eng. Des.*, 2002, vol. 61–62, pp. 129–134.

13. Mazul, I., Giniyatulin, R., Komarov, V., et al., Manufacturing and testing of ITER divertor gas box liners, in *Proc. 20 Symp. on Fusion Technology*, Marseille, France, 1998.

14. Rödig, M., Bobin-Vastra, I., Cox, S., Escourbiac, F., Gervash, A., Kapoustina, A., Kuehnlein, W., Kuznetsov, V., Merola, M., Nygren, R., and Youchison, D.L., Testing of actively cooled mockups in several high heat flux facilities – an international round robin test, *Fusion Eng. Des.*, 2005, vols. 75–79, pp. 303–306.

15. Makhlaj, V.A., Garkusha, I.E., Aksenov, N.N., Kulik, N.V., Landman, I.S., Linke, J., Medvedev, A.V., Malykhin, S.V., Chebotarev, V.V., Pugachev, A.T., and Tereshin, V.I., High heat flux plasma testing of ITER divertor materials under ELM relevant conditions in QSPA Kh-50, *Vopr. At. Nauki Tekhn., Ser. Fiz. Plasmy*, 2010, no. 6, pp. 57–59. http://vant.kipt. kharkov.ua/TABFRAME.html

16. Thomser, C., Linke, J., Matthews, G., Riccardo, V., Schmidt, A., and Vasechko, V., Tungsten coatings under fusion relevant heat loads, *Problems At. Sci. Technol.*, 2010, no. 6, pp. 54–56. http://vant.kipt.kharkov.ua/TABFRAME.html

17. Maslyaev, S.A., Pimenov, V.N., Gribkov, V.A., and Demin, A.S., Damage of Chrome–manganese steels by pulsed fluxes of ions and dense plasma under their separate action on the material in the "Plasma focus" setup, *Inorg. Mater.: Appl. Res.*, 2011, vol. 2, pp. 445–451.

18. Gribkov, V.A., Demin, A.S., Demina, E.V., Dubrovsky, A.V., Karpinsky, L., Maslyaev, S.A., Pimenov, V.N., Padukh, M., and Scholz, M., Physical processes of the interaction of ion and plasma streams with a target surface in a dense plasma focus device, *Plasma Phys. Rep.,* 2012, vol. 38, pp. 1082–1089.

19. *Physical Values. A Handbook*, Grigoriev, I.S. and Meylikhov, E.Z., Eds., Moscow: Energoatomizdat, 1991.

20. Gribkov, V.A., Pimenov, V.N., Roschupkin, V.V., Maslyaev, S.A., Demina, E.V., Lyakhovitsky, M.M., Dubrovsky, A.V., Sasinovskaya, I.P., Chernyshova, M., Scholz, M., Crespo, M.L., Chicutin, A., and Tuniz, C., Irradiation of austenitic steel 10Cr12Mn14Ni4AlMo and titanium alloy Ti–Al–V by pulsed streams of fast nitrogen ions and plasma in a dense plasma focus device, *Nukleonika*, 2012, vol. 57, pp. 291–295.

Translated by K. Utegenov